Received: 24 September 2023 | Revised: 9 April 2024 | Accepted: 28 May 2024

Research Article
Journal of Research and Review in Science
130-146, Volume 11, June 2024
DOI:

ORIGINAL RESEARCH

NODE VITALITY MODEL FOR PARCELLATION OF HUMAN BRAIN FUNCTIONAL MAGNETIC RESONANCE IMAGES

Adam F. Zubair[1], Benjamin S. Aribisala[1], Oluwatoyin A. Enikuomehin[1], Micheal Adenibuyan[2]

[1]*Department of Computer Science, Faculty of Science, Lagos State University, Nigeria*

[2]*Bells University of Technology, Ota. Ogun State. Nigeria*

Correspondence
Adam Folohunsho Zubair, [1]Department of Computer Science, Faculty of Science, Lagos State University, Nigeria.
Email:adam.zubair@lasu.edu.ng

Funding information
NIL

Abstract:

Introduction: One of the methods for investigating brain activity is called functional magnetic resonance imaging (fMRI), and research has shown that it has great potential for use in clinical applications. However, some of the inconsistent findings reported by several research place some limitations on fMRI. The absence of accepted and standardized techniques for evaluating fMRI data is one of the potential causes of the problem. To solve this issue, a standardized parcellation model is desirable.

Aims: In this paper, we evaluated the performance of a novel parcellation framework called the Node Vitality Model (NVM) for fMRI image region of interest definition using the anatomical, functional, and network features of the brain.

Materials and Methods: The model was evaluated using both real data made up of 50 images of the human brain and simulated data created using standard graph methods. Measures of segregation using clustering, resilience using global efficiency, and integration using assortativity were the metrics used to assess the vitality of the brain nodes.

Results: According to the findings, assortativity varied between 0.0022 and 0.1394, clustering varied between 0.5267 and 0.9083, and global efficiency varied between 0.5172 and 0.9167. Only 80 of the 132 nodes taken into consideration in the majority rule's final analysis were found to be significant, and this information was used to construct a brain network. The resulting graph was then used to re-parcellate the brain network using a reverse Engineering approach.

Conclusion: This study showed that the node vitality model has good promise for parcellating fMRI data considering anatomical, functional and network features of the brain.

To Keywords: brain, fMRI, graph theory, parcellation

All co-authors agreed to have their names listed as authors.

1. INTRODUCTION

The investigation of functional connectivity and brain networks in the human brain using functional magnetic resonance imaging (fMRI) has become crucial in neuroscience [1]. The method measures the temporal correlation between several brain regions within a single person over time utilizing task-based time course data acquired via a Blood Oxygenation Level Dependent contrast (BOLD) [2]. Connectivity associations offer crucial diagnostic information for illnesses of the central nervous system. Because of its adaptability, fMRI has been used extensively in neuroscience for studying schizophrenia [6, 7], bipolar disease [6, 8], the link between connectivity and behavior [5, 4], and brain connectivity in different brain states [3, 4].

There have been a number of approaches proposed for processing fMRI data, including as the seed methods [7], principal component analysis [8], independent component analysis [9], and clustering [10]. Although the outcomes of these methods have been encouraging, there is no universal agreement on the best way for data analysis [11, 12]. The potential diagnostic or prognostic significance of fMRI data is diminished by the lack of a standardized technique of processing, and it this has been suggested to be the cause of conflicting results in its clinical uses [13]. In order to establish a framework for the application of fMRI in the early and improved diagnosis of brain-related disorders, the development of a robust and standardized mathematical model for data processing is necessary.

Many analyses of brain networks have used graph theory with great success [14]. This method models the brain as a network or graph, G(N, M), with N "nodes" connected by M "edges". The graph's nodes often represent various anatomical or functional parts of the brain, while the graph's edges show how these regions interact with one another. This model makes it possible to analyze the topology and dynamics of brain networks using a wide range of mathematical tools and theoretical ideas. [15-19]. A number of metrics for assessing network features are provided by graph theory [20], such as small worldness [21], modularity [22], global efficiency [23], clustering coefficient [18], and hierarchical structure [18]. These quantitative network features have been shown to alter throughout normal development [24], aging [22, 25, 26], and a number of neurological and neuropsychiatric illnesses, including Alzheimer's disease (AD) [27] and late-life depression (LLD) [7, 28].

The individual voxels of the brain imaging dataset (voxel-based representation) or the mean values calculated from a group of voxels can both be used to form the nodes of an fMRI brain graph (region-based representation). The region based (ROI) technique sums voxel values over a range of voxels, resulting in higher SNR, whereas analysis using the voxel based (VB) approach is undertaken on a single voxel basis, resulting in low inherent Signal to Noise Ratio (SNR) [29, 30]. As a result, the mean values calculated from a specific region of interest are frequently used to represent the nodes of an fMRI brain graph [31].

The proper designation of brain areas to represent the network nodes is one of the main methodological issues of fMRI graph analysis [13, 32, 33]. The data-driven method, which is not dependent on past knowledge, is an alternative to the model-based method, which is the universal method of defining regions of interest [10, 13, 16, 18, 19, 22, 24, 27, 34-40]. When utilized to detect the fMRI experimental effect, it has been shown that the model-based approach performs better than the data-driven technique [41]. Previous research has demonstrated that the network's organizational properties change depending on the template selected [33, 42]. The Automated Anatomical Labeling (AAL) toolkit [44], the Freesurfer software [45], and the Automatic Nonlinear Image Matching and Automatic Labeling algorithm (ANIMAL) atlas [43] are the most often used templates. The fMRI brain data from each individual is divided into various areas using these templates. Following that, network nodes and edges are formed using pairwise correlation and regional means, respectively. Although this strategy has been quite effective, it has the following drawbacks:

a. Given the lack of distinct macroscopic borders that can be utilized to distinguish between adjacent regions, there is no reliable gold standard for ROI. As a result, the criteria are arbitrary and different for each template. Even after data is translated into a standard space, there is still a significant amount of diversity in terms of individual brain structure.

b. The quantity of voxels within a region cannot be determined in a methodical manner. The current range of this quantity, which affects network organizational factors, is between 10 and 1000 [10, 42].
c. Regions are frequently chosen to be as big as possible (to maximize SNR). Therefore, it is likely that they incorporate signals from several functional sub-regions, which can make it more difficult to understand the results or potentially cause partial volume inaccuracies 32].

2. MATERIAL AND METHODS

The interconnected issues in Section 1 are challenges for analyzing fMRI brain data, which adds to the unreplicability of fMRI data analysis. This means that a model that can effectively divide fMRI brain data into various standard regions must be developed.

Here, we offer a framework for an fMRI analysis model. It will be unnecessary to select a certain number of pixels for each zone because the model uses the anatomical, functional, and network aspects of the brain to group only related pixels into a region.

2.1 Novel Vitality Model

The model was built on several network features, better measurements based on single attributes like the Canonical correlation-based [38] measure, the Modularity [47] measure, and the Normalized Cut [46] metric. The edges of the network will be based on the wavelet correlation coefficient, which has been shown to perform better than Pearson correlation or other time-dependent correlation coefficients [34]. The network nodes will be the mean values from each ROI.
The Node vitality measure algorithm is inspired by research that worked on modelling the impact of lesions on the human brain [10]. The study used graph theory to simulate the presence of brain lesions in order to measure network resilience.

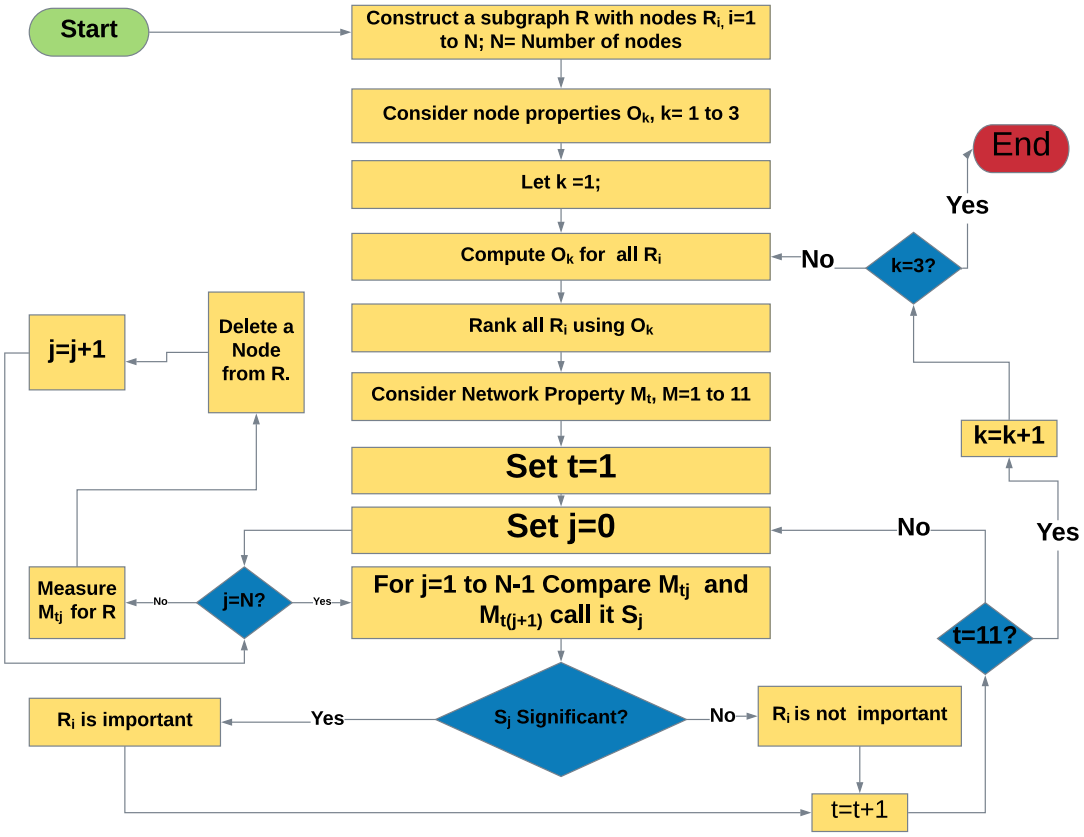

Figure 1: Node Vitality Algorithm

The Node Vitality Measure Algorithm (see Figure 2) applies the idea of quantifying the robustness of brain networks to a node's significance within a network in this project. In essence, it involves taking a node (or a set of nodes) out of a network and comparing how the network behaves (like connectedness) before and after the node is gone. A node is significant if it engages in numerous node interactions, supports node integration, and contributes significantly to the network's resistance to changes

Consequently, the loss of a key node will cause a substantial alteration in the network's characteristics. For instance, removing a node from a network that connects a lot of other nodes will drastically diminish connectivity. The node is not vital and shouldn't be in that region, so it is separated from that region if it is removed with no discernible impact on the network attributes. In order to divide a specific anatomical region into smaller ones, all nodes within that region will be removed.

2.2 Novel Removal Approach

Localized deletion or sequential single node deletion can both be used to remove nodes. Sequential single node elimination involves removing each node one at a time until only one is left. Additionally, a group of nodes are eliminated at a time in localized deletion. What determines which node (or set of nodes) to be picked for removal, regardless of whether a sequential approach or localized technique is used, is a crucial subject. There are two ways to achieve this; The first is targeted node selection, which involves choosing a node for removal based on a metric, like the node's degree.

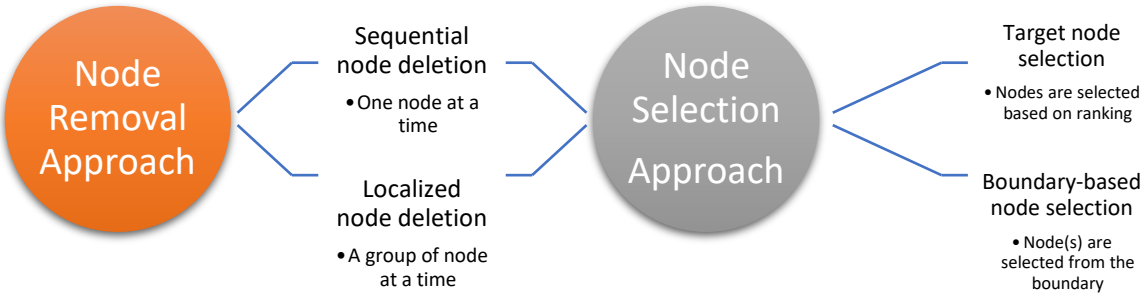

Figure 2: Node Removal Approach

The four potential routes to which a node can be removed based on a certain sort of selection are shown in Figure 2. These four possible channels are:

i. Sequential node deletion using target node selection.
ii. Sequential node deletion using boundary-based node selection.
iii. Localized node deletion using target node selection.
iv. Localized node deletion using boundary-based node selection.

2.3 Data

Two datasets were considered; namely simulated data and real data

2.3.1 Simulated Data

The simulated data, which served as the initial basis for assessing the performance of the suggested algorithm, was produced arbitrarily in form of a graph with nodes resembling a typical brain graph. The created simulated data had 746 edges and 71 nodes (see Figure 3).

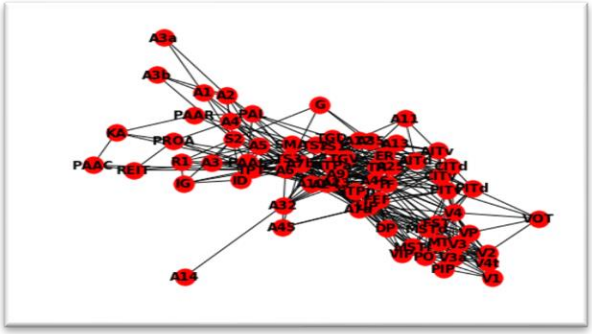

Figure 3: Simulated Data (Subgraph)

2.3.2 Real Data

The real data utilized in the experiment was obtained from the 1000 Functional Connectomes Project, an fMRI archive. An unrestricted public release of more than 1200 functional MRI (fMRI) datasets that were separately obtained at 33 sites is known as the "1000 Functional Connectomes" Project. Every dataset was freely available to the public [50]. The dataset contains information about each participant's age, sex, and imaging center, but the participants' identities are kept secret.

The dataset under consideration comes from a New York contribution (NYU CSC) to the 1000 Functional Connectomes Project, and it consists of T1 Weighted (Figure 4) and resting state fMRI (Figure 5) scans of 50 subjects (35 men and 15 women) aged 20 to 50 (20-50).

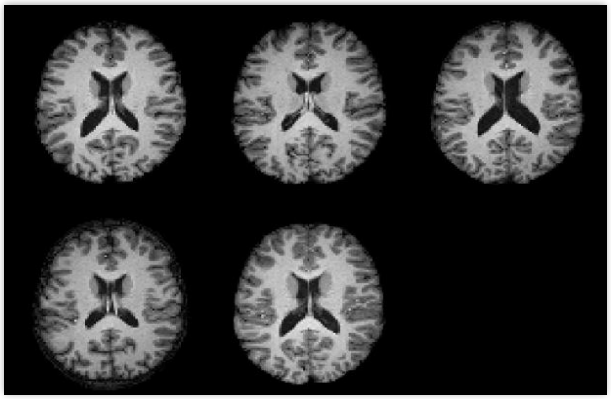

Figure 4: Five Structural brain image (T1 Weighted) from the real data

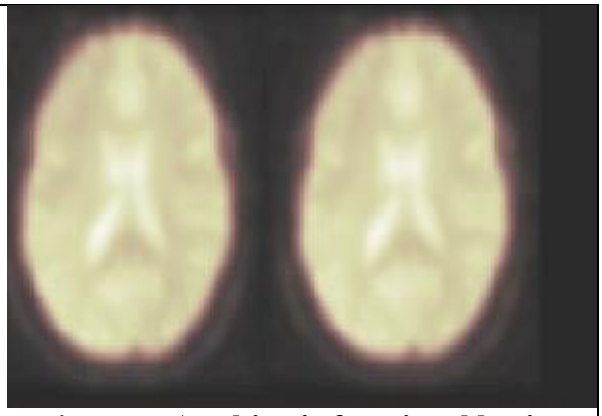

Figure 5: A subject's functional brain Image from the real data

2.4 Experiment

The developed model was tested on the two datasets.

Table 1. Physical, chemical and biological properties of experimental soil (0-20 cm)

S/N	Regions of Interests	Node Label	No of edges
1.	atlas.Cereb8 r (Cerebelum 8 Right)	N1	1
2.	atlas.FO l (Frontal Operculum Cortex Left)	N2	1
3.	atlas.Cereb10 l (Cerebelum 10 Left)	N3	1
4.	atlas.Cereb9 l (Cerebelum 9 Left)	N4	2
5.	atlas.Cereb10 r (Cerebelum 10 Right)	N5	2
6.	atlas.Hippocampus l	N6	2
7.	atlas.Ver3 (Vermis 3)	N7	3
8.	atlas.Caudate r	N8	4
9.	atlas.Cereb7 l (Cerebelum 7b Left)	N9	5
10.	atlas.Ver9 (Vermis 9)	N10	5
11.	atlas.Cereb3 r (Cerebelum 3 Right)	N11	5
12.	atlas.aTFusC l (Temporal Fusiform Cortex, anterior division Left)	N12	5
13.	atlas.Ver10 (Vermis 10)	N13	6
14.	atlas.Ver8 (Vermis 8)	N14	6
15.	atlas.aTFusC r (Temporal Fusiform Cortex, anterior division Right)	N15	6
16.	atlas.Cereb8 l (Cerebelum 8 Left)	N16	7
17.	atlas.pPaHC l (Parahippocampal Gyrus, posterior division Left)	N17	7
18.	atlas.SCC l (Supracalcarine Cortex Left)	N18	8

19.	atlas.Pallidum l	N19	9
20.	atlas.Caudate l	N20	9
21.	atlas.PP l (Planum Polare Left)	N21	9
22.	atlas.Cereb3 l (Cerebelum 3 Left)	N22	9
23.	atlas.Hippocampus r	N23	10
24.	atlas.aITG l (Inferior Temporal Gyrus, anterior division Left)	N24	10
25.	atlas.Cereb7 r (Cerebelum 7b Right)	N25	10
26.	atlas.pITG r (Inferior Temporal Gyrus, posterior division Right)	N26	11
27.	atlas.aPaHC l (Parahippocampal Gyrus, anterior division Left)	N27	11
28.	atlas.iLOC r (Lateral Occipital Cortex, inferior division Right)	N28	11
29.	atlas.toMTG r (Middle Temporal Gyrus, temporooccipital part Right)	N29	11
30.	atlas.Brain-Stem	N30	11
31.	atlas.Accumbens r	N31	12
32.	atlas.toITG l (Inferior Temporal Gyrus, temporooccipital part Left)	N32	12
33.	atlas.pPaHC r (Parahippocampal Gyrus, posterior division Right)	N33	13
34.	atlas.Pallidum r	N34	13
35.	atlas.Cereb9 r (Cerebelum 9 Right)	N35	13
36.	atlas.ICC l (Intracalcarine Cortex Left)	N36	13
37.	atlas.Accumbens l	N37	13
38.	atlas.toITG r (Inferior Temporal Gyrus, temporooccipital part Right)	N38	14
39.	atlas.sLOC l (Lateral Occipital Cortex, superior division Left)	N39	14
40.	atlas.Cereb2 r (Cerebelum Crus2 Right)	N40	14
41.	atlas.Putamen r	N41	15
42.	atlas.Putamen l	N42	15
43.	atlas.Cereb45 r (Cerebelum 4 5 Right)	N43	16
44.	atlas.aMTG r (Middle Temporal Gyrus, anterior division Right)	N44	16
45.	atlas.pSTG l (Superior Temporal Gyrus, posterior division Left)	N45	16
46.	atlas.SPL l (Superior Parietal Lobule Left)	N46	16
47.	atlas.Cuneal l (Cuneal Cortex Left)	N47	17
48.	atlas.pITG l (Inferior Temporal Gyrus, posterior division Left)	N48	17
49.	atlas.PaCiG l (Paracingulate Gyrus Left)	N49	17
50.	atlas.FO r (Frontal Operculum Cortex Right)	N50	17
51.	atlas.IFG oper l (Inferior Frontal Gyrus, pars opercularis Left)	N51	17
52.	atlas.SPL r (Superior Parietal Lobule Right)	N52	18
53.	atlas.IFG tri l (Inferior Frontal Gyrus, pars triangularis Left)	N53	18
54.	atlas.aPaHC r (Parahippocampal Gyrus, anterior division Right)	N54	18
55.	atlas.OP l (Occipital Pole Left)	N55	18
56.	atlas.Amygdala r	N56	18
57.	atlas.SCC r (Supracalcarine Cortex Right)	N57	18
58.	atlas.sLOC r (Lateral Occipital Cortex, superior division Right)	N58	19
59.	atlas.aSTG r (Superior Temporal Gyrus, anterior division Right)	N59	19
60.	atlas.iLOC l (Lateral Occipital Cortex, inferior division Left)	N60	19

61.	atlas.SMA r (Juxtapositional Lobule Cortex -formerly Supplementary Motor Cortex- Right)	N61	19
62.	atlas.OFusG l (Occipital Fusiform Gyrus Left)	N62	19
63.	atlas.aSMG l (Supramarginal Gyrus, anterior division Left)	N63	19
64.	atlas.OFusG r (Occipital Fusiform Gyrus Right)	N64	20
65.	atlas.HG l (Heschl's Gyrus Left)	N65	20
66.	atlas.pSTG r (Superior Temporal Gyrus, posterior division Right)	N66	20
67.	atlas.Ver6 (Vermis 6)	N67	20
68.	atlas.FP l (Frontal Pole Left)	N68	20
69.	atlas.MedFC (Frontal Medial Cortex)	N71	20
70.	atlas.pTFusC l (Temporal Fusiform Cortex, posterior division Left)	N72	21
71.	atlas.Thalamus r	N73	21
72.	atlas.Cuneal r (Cuneal Cortex Right)	N74	21
73.	atlas.PO r (Parietal Operculum Cortex Right)	N75	21
74.	atlas.toMTG l (Middle Temporal Gyrus, temporooccipital part Left)	N76	21
75.	atlas.SubCalC (Subcallosal Cortex)	N78	21
76.	atlas.PP r (Planum Polare Right)	N79	21
77.	atlas.pTFusC r (Temporal Fusiform Cortex, posterior division Right)	N80	22
78.	atlas.ICC r (Intracalcarine Cortex Right)	N82	22
79.	atlas.LG r (Lingual Gyrus Right)	N83	22
80.	atlas.TOFusC r (Temporal Occipital Fusiform Cortex Right)	N84	22
81.	atlas.HG r (Heschl's Gyrus Right)	N85	22
82.	atlas.aITG r (Inferior Temporal Gyrus, anterior division Right)	N86	23
83.	atlas.Ver7 (Vermis 7)	N87	23
84.	atlas.OP r (Occipital Pole Right)	N88	23
85.	atlas.aSTG l (Superior Temporal Gyrus, anterior division Left)	N89	24
86.	atlas.MidFG r (Middle Frontal Gyrus Right)	N90	25
87.	atlas.AG l (Angular Gyrus Left)	N91	25
88.	atlas.FOrb l (Frontal Orbital Cortex Left)	N92	25
89.	atlas.AG r (Angular Gyrus Right)	N93	25
90.	atlas.PC (Cingulate Gyrus, posterior division)	N94	26
91.	atlas.Ver45 (Vermis 4 5)	N95	26
92.	atlas.aSMG r (Supramarginal Gyrus, anterior division Right)	N96	26
93.	atlas.AC (Cingulate Gyrus, anterior division)	N97	26
94.	atlas.FOrb r (Frontal Orbital Cortex Right)	N98	26
95.	atlas.LG l (Lingual Gyrus Left)	N99	26
96.	atlas.pSMG l (Supramarginal Gyrus, posterior division Left)	N100	27
97.	atlas.SMA L(Juxtapositional Lobule Cortex -formerly Supplementary Motor Cortex- Left)	N101	27
98.	atlas.pMTG l (Middle Temporal Gyrus, posterior division Left)	N102	28
99.	atlas.PaCiG r (Paracingulate Gyrus Right)	N103	28
100.	atlas.pSMG r (Supramarginal Gyrus, posterior division Right)	N104	29
101.	atlas.TOFusC l (Temporal Occipital Fusiform Cortex Left)	N105	29
102.	atlas.CO r (Central Opercular Cortex Right)	N106	30

103.	atlas.Cereb6 l (Cerebelum 6 Left)	N107	30
104.	atlas.PostCG l (Postcentral Gyrus Left)	N108	30
105.	atlas.aMTG l (Middle Temporal Gyrus, anterior division Left)	N109	30
106.	atlas.IFG tri r (Inferior Frontal Gyrus, pars triangularis Right)	N110	30
107.	atlas.SFG r (Superior Frontal Gyrus Right)	N111	30
108.	atlas.PO l (Parietal Operculum Cortex Left)	N112	30
109.	atlas.SFG l (Superior Frontal Gyrus Left)	N113	31
110.	atlas.MidFG l (Middle Frontal Gyrus Left)	N114	31
111.	atlas.TP r (Temporal Pole Right)	N115	32
112.	atlas.IFG oper r (Inferior Frontal Gyrus, pars opercularis Right)	N116	33
113.	atlas.CO l (Central Opercular Cortex Left)	N117	33
114.	atlas.Thalamus l	N118	33
115.	atlas.PT l (Planum Temporale Left)	N119	34
116.	atlas.Precuneous (Precuneous Cortex)	N120	34
117.	atlas.Cereb2 l (Cerebelum Crus2 Left)	N121	34
118.	atlas.PreCG r (Precentral Gyrus Right)	N122	35
119.	atlas.FP r (Frontal Pole Right)	N123	35
120.	atlas.PreCG l (Precentral Gyrus Left)	N124	35
121.	atlas.pMTG r (Middle Temporal Gyrus, posterior division Right)	N125	37
122.	atlas.TP l (Temporal Pole Left)	N126	38
123.	atlas.PostCG r (Postcentral Gyrus Right)	N127	38
124.	atlas.PT r (Planum Temporale Right)	N128	38
125.	atlas.IC l (Insular Cortex Left)	N129	39
126.	atlas.Cereb1 l (Cerebelum Crus1 Left)	N130	39
127.	atlas.Cereb6 r (Cerebelum 6 Right)	N131	39
128.	atlas.Cereb45 l (Cerebelum 4 5 Left)	N132	46

2.4.1 Node Significance indicator

The selected metrics were used to generate a node significant indicator that specifies the significant of a node by considering and comparing the changing in the values of the metric before and after a node is removed from the subgraph **R**. A decrease in the value of each metric whenever a node is removed indicates significance and an increase in the value indicates insignificance. The results of the three metrics combined to form a logical decision table that indicates the significance of a node (see **Table** Error! No text of specified style in document.**.1**)

Table Error! No text of specified style in document.**.1 Node Significance Indicator**

S/N	Assortativity	Clustering	Global Efficiency	Node Significance
1.	Increase	Increase	Increase	Insignificant
2.	Increase	Increase	Decrease	Insignificant
3.	Increase	Decrease	Increase	Insignificant

4.	Decrease	Increase	Increase	Insignificant
5.	Increase	Decrease	Decrease	Significant
6.	Decrease	Increase	Decrease	Significant
7.	Decrease	Decrease	Increase	Significant
8.	Decrease	Decrease	Decrease	Significant

2.4.2 Voting Rule

In order to reconstruct a new brain model from the node significance recordings across multiple subjects' brain, a classification strategy is required to determine which nodes will be retained and we nodes are to be merged. Owing to this, a **majority voting rule** will be employed. In majority rule each individual classifier represents one score that is either as a whole assigned to one class label or divided into several labels. The label, which receives more than half of the total scores, is taken as the final result [55-56].
The majority voting rule has been proved to be effective in different cases of fusing and labelling brain segmentations [57-59]

3. RESULTS AND DISCUSSION

3.1 Results

The evaluation of the Node Vitality Model (NVM) was conducted using both simulated and real fMRI datasets to assess its efficacy in brain network parcellation. The results were analyzed based on three key network metrics: segregation, integration, and resilience.

3.1.1 Measure of Segregation

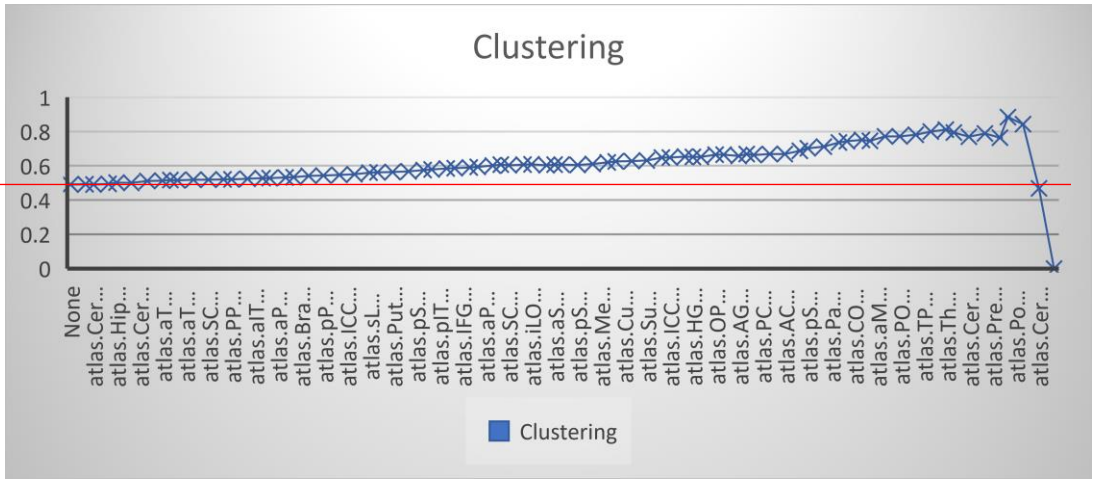

Figure 6: Line Graph showing changes in the clustering metric triggered by node removal

The clustering coefficient was used to evaluate the segregation properties of the brain network. As shown in Figure 6, the clustering values for different nodes were assessed before and after their removal. The red boundary line represents the initial clustering coefficient before node removal. Any node removal that resulted in a decrease in clustering value below this boundary was considered significant. The results revealed that several nodes exhibited substantial reductions in clustering coefficient, indicating their strong contribution to network segregation.

3.1.2 Measure of Integration

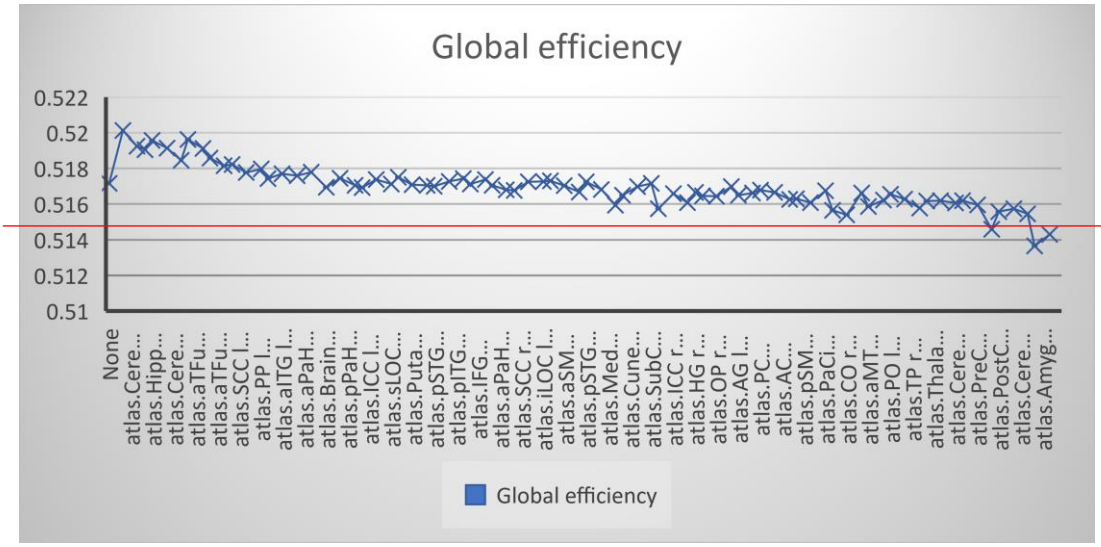

Figure 7: Line Graph showing changes in the global efficiency metric triggered by node removal

Global efficiency was employed to measure the level of integration within the brain network. Figure 7 illustrates the variations in global efficiency values triggered by the removal of individual nodes. Similar to the clustering analysis, the red line serves as the reference point for the pre-removal efficiency. Nodes whose removal led to a significant drop in global efficiency were deemed critical for network integration. The findings demonstrated that the NVM successfully identified key nodes that enhance the interconnectedness of brain regions, thereby reinforcing network integration.

3.1.3 Measure of Resilience

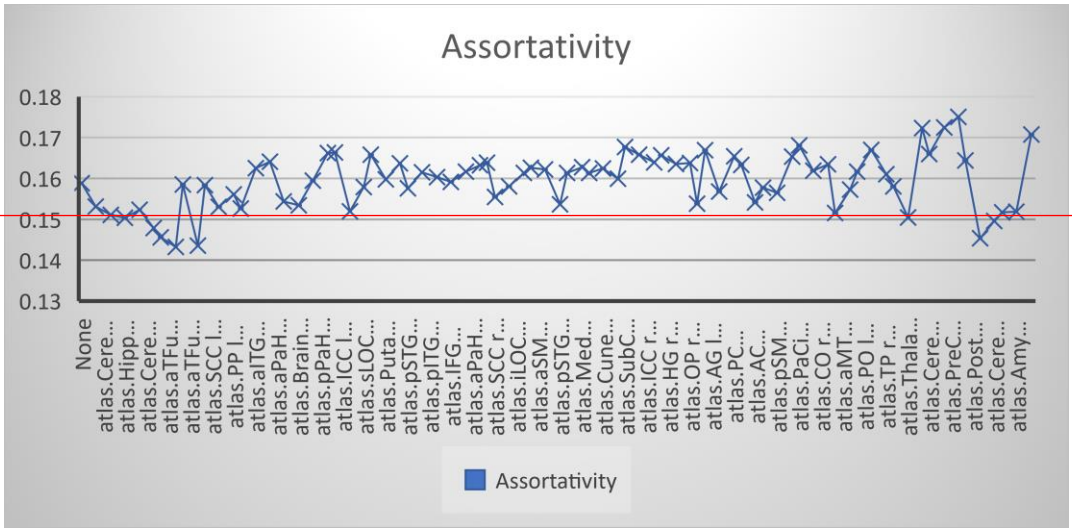

Figure 8: Line Graph showing changes in the assortatvity metric triggered by node removal

Resilience was evaluated using the assortativity metric, which reflects the tendency of nodes to connect with similar nodes. Figure 8 presents the changes in assortativity values following node removal. The results show that certain nodes played a crucial role in maintaining the network's resilience, as their removal caused a noticeable decrease in assortativity. Nodes whose removal had minimal impact on assortativity were classified as less significant and were candidates for merging

3.2 Discussion

Here, the implications of putting this research's technique into practice are explored. Accordingly, the implications and reasons of the experiment's findings are stressed.

3.2.1 Implication of results

The graph metrics were obtained after each node was successively eliminated to ascertain its significance. According to the findings, assortativity varied between 0.0022 and 0.1394, clustering varied between 0.5267 and 0.9083, and overall effectiveness varied between 0.5172 and 0.9167.

The node that has the status "Merge" is combined with its neighbours' nodes that have the most edges and similar brain functions. The regions that resulted from the merging sequence are displayed.

3.2.2 Strenghts and Weaknesses

The fact that 52 nodes were combined and 80 nodes were kept does not affect the integrity of the brain network because it is merely a reassignment of regions to be included in other nearby regions that share a high level of connection. Therefore, having fewer nodes means that there is a dramatic increase in connection between brain regions and a consequent reduction in the segregation between previously distant regions.

The node vitality algorithm-generated brain graph was compared to the prior network metrics of the brain graph that were collected using an atlas. Our finding (see Table 2) demonstrates that after the non-significant nodes were merged with the retained nodes, the network metric with regards to resilience, segregation, and integration has a noticeable improvement across most of the subjects. Due to its higher level of integrated sections, the newly developed brain network becomes more sensitive to changes, which will better tracking of both minor and significant flaws in the brain regions.

Table 2. Network Performance of parcellation result

S/N	Subjects	Assortativity		Clustering		Global Efficiency	
		Merge Effect		Merge Effect		Merge Effect	
		Before	After	Before	After	Before	After
1.	Subject 1	0.311502	0.344501	0.483007	0.5311	0.51492	0.52135
2.	Subject 2	0.30615	0.329682	0.476801	0.47891	0.50345	0.56712
3.	Subject 3	0.314424	0.401048	0.46205	0.516771	0.544947	0.567226
4.	Subject 4	0.374363	0.459906	0.514738	0.585986	0.563227	0.587811
5.	Subject 5	0.312828	0.368161	0.514486	0.568022	0.56724	0.603792
6.	Subject 6	0.363692	0.454385	0.478571	0.544347	0.506079	0.545726
7.	Subject 7	0.386139	0.457272	0.482184	0.533078	0.589733	0.619357
8.	Subject 8	0.382528	0.436118	0.486087	0.542555	0.53586	0.574051
9.	Subject 9	0.366856	0.425141	0.46445	0.514577	0.574879	0.622306
10.	Subject 10	0.336813	0.402709	0.460017	0.548403	0.599942	0.634521
11.	Subject 11	0.378585	0.465928	0.487119	0.552857	0.530345	0.57993
12.	Subject 12	0.311474	0.379887	0.508827	0.591999	0.520402	0.545346
13.	Subject 13	0.341475	0.414638	0.471115	0.569332	0.548645	0.572307
14.	Subject 14	0.3715	0.42218	0.497902	0.57909	0.542894	0.5682
15.	Subject 15	0.300356	0.397988	0.462269	0.557268	0.578539	0.620174
16.	Subject 16	0.355757	0.450832	0.516455	0.568045	0.547032	0.596431
17.	Subject 17	0.342448	0.417125	0.467121	0.525014	0.55526	0.600021
18.	Subject 18	0.377373	0.442056	0.469771	0.536946	0.567461	0.589868
19.	Subject 19	0.309714	0.387828	0.453291	0.548148	0.575991	0.613694
20.	Subject 20	0.389186	0.461966	0.51899	0.579311	0.572925	0.615253
21.	Subject 21	0.319067	0.380249	0.489227	0.55598	0.589379	0.615561
22.	Subject 22	0.319178	0.402468	0.464107	0.53309	0.505097	0.530379
23.	Subject 23	0.34952	0.409292	0.505155	0.597183	0.567463	0.615543
24.	Subject 24	0.372455	0.45536	0.478102	0.541073	0.529317	0.575966
25.	Subject 25	0.379312	0.451597	0.491345	0.568557	0.586559	0.630959
26.	Subject 26	0.365657	0.437346	0.468464	0.531036	0.572679	0.594004
27.	Subject 27	0.308794	0.369813	0.460701	0.5183	0.544478	0.582385
28.	Subject 28	0.319697	0.386209	0.499777	0.587269	0.574629	0.602452
29.	Subject 29	0.363848	0.452903	0.481362	0.564529	0.525918	0.557531
30.	Subject 30	0.334927	0.407509	0.519797	0.591387	0.528466	0.557867
31.	Subject 31	0.338934	0.413455	0.492443	0.592282	0.593663	0.62129
32.	Subject 32	0.367519	0.440204	0.466628	0.556553	0.591895	0.615589
33.	Subject 33	0.338245	0.437154	0.494443	0.570132	0.519904	0.546347
34.	Subject 34	0.339843	0.396897	0.495276	0.566966	0.510407	0.547113
35.	Subject 35	0.355617	0.421004	0.511199	0.584211	0.558165	0.60102
36.	Subject 36	0.348353	0.438851	0.487638	0.577082	0.506489	0.531036
37.	Subject 37	0.368786	0.454781	0.511031	0.58767	0.585106	0.61071
38.	Subject 38	0.370918	0.446465	0.500297	0.564478	0.522424	0.56667
39.	Subject 39	0.387806	0.451837	0.512203	0.574348	0.581004	0.606272
40.	Subject 40	0.347294	0.411239	0.519597	0.616677	0.548052	0.585269
41.	Subject 41	0.308587	0.387092	0.453271	0.546047	0.514482	0.549332
42.	Subject 42	0.367974	0.452045	0.512289	0.592553	0.553398	0.601827
43.	Subject 43	0.340317	0.420682	0.486577	0.578909	0.555038	0.593346
44.	Subject 44	0.37176	0.452541	0.451431	0.50372	0.58775	0.614837
45.	Subject 45	0.334454	0.390929	0.457525	0.543783	0.570763	0.598752
46.	Subject 46	0.397102	0.46641	0.498342	0.597374	0.598915	0.622774
47.	Subject 47	0.334006	0.408818	0.46813	0.548527	0.583736	0.615149
48.	Subject 48	0.317961	0.384088	0.461453	0.560052	0.597486	0.638197
49.	Subject 49	0.312614	0.401225	0.461431	0.47372	0.533869	0.567436
50.	Subject 50	0.3151	0.30978	0.45680	0.4722	0.5287	0.5455

The findings from the three metrics collectively guided the classification of significant and insignificant nodes. The majority voting rule was applied to determine the final parcellation, leading to the retention of 80 significant nodes and the merging of 52 nodes. Table 2 presents the network performance metrics before and after the application of the NVM across multiple subjects.

The results indicate that the parcellation achieved through the NVM led to an overall improvement in network connectivity. The refined brain network exhibited enhanced integration and resilience, suggesting that the NVM provides a more consistent and biologically meaningful framework for brain parcellation compared to traditional atlas-based approaches.

4. CONCLUSION

This study has revealed that the node vitality measure algorithm is an effective tool for dividing parcellating the brain more uniformly compared to existing arbitrary approaches, due to its consistency of node classification across different subjects. The node vitality measure program can be utilized remotely by any research lead using Google Colab's free source program. The resulting significance of ROIs across multiple subjects can be utilized to evenly partition the brain into relevant regions of interest. To bolster and improve its efficacy, the node vitality model could be expanded to include more than three graph metrics. The addition of additional measures will guarantee a more comprehensive assessment of node significance and classification. Because some research implies that using numerous atlases instead of a single atlas result in more reliable findings, the usage of multiple atlases for the initial parcellation operation can be further investigated. To find the optimal clinical use of the node vitality parcellation model, the medical ramifications of node categorization might be investigated.

ACKNOWLEDGEMENTS

REFERENCES

1. Batista-García-Ramó, K. and C.I.J.B.S. Fernández-Verdecia, *What we know about the brain structure–function relationship.* 2018. **8**(4): p. 39.
2. Saviola, F., et al., *Trait and state anxiety are mapped differently in the human brain.* 2020. **10**(1): p. 1-11.
3. Elam, J.S., et al., *The Human Connectome Project: A retrospective.* 2021. **244**: p. 118543.
4. Azevedo, F.A., et al., *Equal numbers of neuronal and nonneuronal cells make the human brain an isometrically scaled-up primate brain.* 2009. **513**(5): p. 532-541.
5. Rasmussen, M.K., H. Mestre, and M.J.P.R. Nedergaard, *Fluid transport in the brain.* 2022. **102**(2): p. 1025-1151.
6. Soomro, T.A., et al., *Image Segmentation for MR Brain Tumor Detection Using Machine Learning: A Review.* 2022.
7. de Villiers, R., *The Human Brain–Cortex, Lobes, Neural Networks and Problem Solved!*, in *The Handbook of Creativity & Innovation in Business*. 2022, Springer. p. 25-49.
8. Westbrook, C., *Handbook of MRI technique*. 2014: John Wiley & Sons.
9. Majumder, D.K.D. and D. Ray, *Fundamentals of Medical Image Processing Using Matlab* 2022: PHI Learning Pvt. Ltd.
10. Lessard, E.J., *Magnetic Resonance Systems Development for Point-of-Care MRI Platforms.* 2022.
11. de la Encarnación, C., D.J. de Aberasturi, and L.M.J.A.D.D.R. Liz-Marzán, *Multifunctional plasmonic-magnetic nanoparticles for bioimaging and hyperthermia.* 2022: p. 114484.

12. Kvet, M. and K. Matiaško. *Epsilon temporal data in MRI results processing*. in *The 10th International Conference on Digital Technologies 2014*. 2014. IEEE.
13. Eickhoff, S.B., B. Yeo, and S.J.N.R.N. Genon, *Imaging-based parcellations of the human brain.* 2018. **19**(11): p. 672-686.
14. Ogawa, S., et al., *Brain magnetic resonance imaging with contrast dependent on blood oxygenation.* Proceedings of the National Academy of Sciences, 1990. **87**(24): p. 9868-9872.
15. Hay, L., et al., *Functional magnetic resonance imaging (fMRI) in design studies: Methodological considerations, challenges, and recommendations.* 2022. **78**: p. 101078.
16. Tholen, M.G., et al., *Functional magnetic resonance imaging (fMRI) item analysis of empathy and theory of mind.* 2020. **41**(10): p. 2611-2628.
17. Arias, J., et al. *PyHRF: A Python Library for the Analysis of fMRI Data Based on Local Estimation of the Hemodynamic Response Function*. in *16th Python in Science Conference (SciPy 2017)*. 2017.
18. Specht, K.J.F.i.p., *Current challenges in translational and clinical fMRI and future directions.* 2020: p. 924.
19. Vul, E., et al., *Puzzlingly high correlations in fMRI studies of emotion, personality, and social cognition.* 2009. **4**(3): p. 274-290.
20. Turner, B.O., et al., *Small sample sizes reduce the replicability of task-based fMRI studies.* 2018. **1**(1): p. 1-10.
21. Bennett, C.M., M.B. Miller, and G.L.J.N. Wolford, *Neural correlates of interspecies perspective taking in the post-mortem Atlantic Salmon: an argument for multiple comparisons correction.* 2009. **47**(Suppl 1): p. S125.
22. Yang, X., et al., *Blockwise human brain network visual comparison using nodetrix representation.* IEEE transactions on visualization and computer graphics, 2016. **23**(1): p. 181-190.
23. Cole, D.M., S.M. Smith, and C.F. Beckmann, *Advances and pitfalls in the analysis and interpretation of resting-state FMRI data.* Frontiers in systems neuroscience, 2010. **4**: p. 8.
24. Costa, C., et al., *Brain activity during facial processing in autism spectrum disorder: an activation likelihood estimation (ALE) meta-analysis of neuroimaging studies.* 2021.
25. Fornito, A., A. Zalesky, and E.T. Bullmore, *Network scaling effects in graph analytic studies of human resting-state FMRI data.* Frontiers in systems neuroscience, 2010. **4**: p. 22.
26. Wang, J., X. Zuo, and Y. He, *Graph-based network analysis of resting-state functional MRI.* Frontiers in systems neuroscience, 2010. **4**: p. 16.
27. Arslan, S., et al., *Human brain mapping: A systematic comparison of parcellation methods for the human cerebral cortex.* Neuroimage, 2018. **170**: p. 5-30.
28. Salvador, R., et al., *Neurophysiological architecture of functional magnetic resonance images of human brain.* Cerebral cortex, 2005. **15**(9): p. 1332-1342.
29. Albert, R. and A.-L. Barabási, *Statistical mechanics of complex networks.* Reviews of modern physics, 2002. **74**(1): p. 47.
30. Bullmore, E. and O. Sporns, *Complex brain networks: graph theoretical analysis of structural and functional systems.* Nature Reviews Neuroscience, 2009. **10**(3): p. 186.
31. Rubinov, M. and O. Sporns, *Complex network measures of brain connectivity: uses and interpretations.* Neuroimage, 2010. **52**(3): p. 1059-1069.
32. Supekar, K., M. Musen, and V. Menon, *Development of large-scale functional brain networks in children.* PLoS biology, 2009. **7**(7): p. e1000157.
33. Meunier, D., et al., *Hierarchical modularity in human brain functional networks.* Frontiers in neuroinformatics, 2009. **3**: p. 37.

34. Buckner, R.L., et al., *Cortical hubs revealed by intrinsic functional connectivity: mapping, assessment of stability, and relation to Alzheimer's disease.* Journal of neuroscience, 2009. **29**(6): p. 1860-1873.
35. Zalesky, A., et al., *Whole-brain anatomical networks: does the choice of nodes matter?* Neuroimage, 2010. **50**(3): p. 970-983.
36. Achard, S., et al., *A resilient, low-frequency, small-world human brain functional network with highly connected association cortical hubs.* Journal of Neuroscience, 2006. **26**(1): p. 63-72.
37. Aubert-Broche, B., et al., *Clustering of atlas-defined cortical regions based on relaxation times and proton density.* Neuroimage, 2009. **47**(2): p. 523-532.
38. Chen, Z.J., et al., *Revealing modular architecture of human brain structural networks by using cortical thickness from MRI.* Cerebral cortex, 2008. **18**(10): p. 2374-2381.
39. Deleus, F. and M.M. Van Hulle, *A connectivity-based method for defining regions-of-interest in fMRI data.* IEEE Transactions on Image Processing, 2009. **18**(8): p. 1760-1771.
40. Estrada, E. and N. Hatano, *Communicability in complex networks.* Physical Review E, 2008. **77**(3): p. 036111.
41. Honey, C., et al., *Predicting human resting-state functional connectivity from structural connectivity.* Proceedings of the National Academy of Sciences, 2009. **106**(6): p. 2035-2040.
42. Eickhoff, S.B., et al., *Connectivity-based parcellation: Critique and implications.* Human brain mapping, 2015. **36**(12): p. 4771-4792.
43. Wang, L., et al., *Altered small-world brain functional networks in children with attention-deficit/hyperactivity disorder.* Human brain mapping, 2009. **30**(2): p. 638-649.
44. Collins, D.L., et al., *Automatic 3-D model-based neuroanatomical segmentation.* Human brain mapping, 1995. **3**(3): p. 190-208.
45. Tzourio-Mazoyer, N., et al., *Automated anatomical labeling of activations in SPM using a macroscopic anatomical parcellation of the MNI MRI single-subject brain.* Neuroimage, 2002. **15**(1): p. 273-289.
46. Fischl, B., et al., *Automatically parcellating the human cerebral cortex.* Cerebral cortex, 2004. **14**(1): p. 11-22.
47. Biswal, B.B., et al., *Toward discovery science of human brain function.* Proceedings of the National Academy of Sciences, 2010. **107**(10): p. 4734-4739.
48. Mier, W. and D.J.F.i.h.n. Mier, *Advantages in functional imaging of the brain.* 2015. **9**: p. 249.
49. Cover, G., et al., *Computational methods for corpus callosum segmentation on MRI: A systematic literature review.* 2018. **154**: p. 25-35.
50. Mennes, M., et al., *Making data sharing work: the FCP/INDI experience.* Neuroimage, 2013. **82**: p. 683-691.
51. Whitten, L.A., *Functional Magnetic Resonance Imaging (fMRI): An Invaluable Tool in Translational Neuroscience.* 2012.
52. Zhang, S., et al., *Characterizing and differentiating task-based and resting state fMRI signals via two-stage sparse representations.* 2016. **10**(1): p. 21-32.
53. Stolz, B.J., et al., *Topological data analysis of task-based fMRI data from experiments on schizophrenia.* 2021. **2**(3): p. 035006.
54. Sighinolfi, G., et al., *What Can Resting-State fMRI Data Analysis Explain about the Functional Brain Connectivity in Glioma Patients?* 2022. **8**(1): p. 267-280.
55. Xu, L., et al., *Methods of combining multiple classifiers and their applications to handwriting recognition.* 1992. **22**(3): p. 418-435.
56. Mossel, E.J.B.o.t.A.M.S., *Probabilistic view of voting, paradoxes, and manipulation.* 2022. **59**(3): p. 297-330.

57. Rohlfing, T., et al., *Evaluation of atlas selection strategies for atlas-based image segmentation with application to confocal microscopy images of bee brains.* 2004. **21**(4): p. 1428-1442.
58. Heckemann, R.A., et al., *Automatic anatomical brain MRI segmentation combining label propagation and decision fusion.* 2006. **33**(1): p. 115-126.
59. Richiardi, J., et al., *Decoding brain states from fMRI connectivity graphs.* 2011. **56**(2): p. 616-626